Thermal Science and Engineering Progress 59 (2025) 103342

Contents lists available at ScienceDirect

Thermal Science and Engineering Progress

journal homepage: www.sciencedirect.com/journal/thermal-science-and-engineering-progress

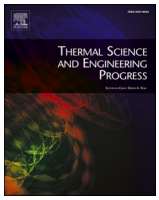

Liquid fuel evaporation under entrained flow gasification conditions – Insights for burner development☆

Manuel Haas [a,*], Sabine Fleck [a], Tobias Jakobs [a], Thomas Kolb [a,b]

[a] Institute for Technical Chemistry Department of Gasification Technology (ITC-vgt) Karlsruhe Institute of Technology (KIT) Eggenstein-Leopoldshafen Germany
[b] Engler-Bunte-Institut Department of Fuel Technology Karlsruhe Institute of Technology (KIT) Karlsruhe Germany

ARTICLE INFO

Keywords:
Entrained Flow Gasification
Evaporation
Flame Structure
Fuel Conversion
Syngas
Inverse Diffusion Flame
Carbon Cycle

ABSTRACT

This study investigates the evaporation of a liquid surrogate fuel in the burner near region of an atmospheric pressure Entrained Flow Gasification (EFG) unit. Fuel evaporation is compared for two twin-fluid atomizer nozzles with different gas exit area under identical gas and liquid mass flow. PDA and Fuel-Tracer LIF are used to measure droplet size, droplet velocity and fuel spray distribution under reacting conditions for both cases while OH-LIF is used to measure the flame structure. A 2-Phase Free Jet Model (2-Ph-FJM) is applied in a sensitivity study on the influence of gas momentum flow, spray angle and droplet size on fuel evaporation in the high temperature oxidation zone. The impact of the liquid evaporation model is investigated by comparing two model approaches. Model results are used to interpret the experimental data and to derive an understanding of the fuel conversion processes in the investigated flame. A major portion of fuel was found to evaporate outside the flame boundaries in both investigated cases. Data indicates a strong impact of droplet residence time and spray parameters on the amount of fuel evaporation within the EFG flame. The 2-Ph-FJM shows the capability to identify beneficial and detrimental parameter spaces for fuel evaporation in the flame. With further understanding of by-product formation under EFG conditions, the detailed experimental data and the insights gained from the numerical study are a useful basis for further development of EFG burners and to define boundary conditions for CFD reactor simulations.

1. Introduction

Processes for the conversion of waste based biogenic and anthropogenic feedstocks into platform chemicals are needed in order to achieve a transition from a linear to a circular economy with closed material cycles. High-pressure Entrained Flow Gasification (HP-EFG) can serve as an enabling technology for a closed carbon cycle because of its ability to generate a high quality syngas from waste based fuels with a wide spectrum of contaminants, e.g. pyrolysis oil derived from mixed plastic wastes. As shown by various authors [1–6], fuel conversion in the burner near region of entrained flow gasifiers is characterized by a complex interaction of different sub-processes that influence fuel conversion and syngas quality. For design and scale up of efficient and fuel flexible EFG-processes, a detailed understanding of the fuel conversion processes in the burner near region is necessary.

EFG reactors typically use external mixing twin fluid burner nozzles to feed fuel and gasification medium to the reactor. The high momentum of the gasification medium disintegrates the liquid fuel phase into a spray, with local mass flux and droplet size depending on nozzle geometry and operating conditions. Fuel spray conversion under combustion conditions has been extensively studied [7–12]. Under combustion conditions it is known that droplet diameter [13–15], spatial spray distribution [14], inter-droplet distance [10,11] and gas phase mixing [16] can heavily impact fuel burnout and emission of soot and unburned hydrocarbons. However, few studies explicitly investigate the influence of these parameters on the fuel conversion processes in EFG, which is caused by diagnostic difficulties under the harsh conditions in EFG reactors, the complex situation being difficult to reproduce in laboratory systems and the lack of validated models of the burner near zone.

A key difference between the situation in common spray combustion systems and EFG reactors is the presence of a combustible atmosphere surrounding the jet that leads to the stabilization of an inverse gas diffusion flame superimposed by a liquid fuel spray. Under EFG

☆ This article is part of a special issue entitled: 'INFUB 14' published in Thermal Science and Engineering Progress.

* Corresponding author.
E-mail address: manuel.haas@kit.edu (M. Haas).

https://doi.org/10.1016/j.tsep.2025.103342
Received 1 December 2024; Received in revised form 29 January 2025; Accepted 30 January 2025
Available online 31 January 2025

conditions, the high momentum jet of oxygen rich gasification medium entrains hot ambient syngas, which stabilizes a high temperature oxidation zone near the burner nozzle [1,17]. The heat release in this zone leads to heat up, evaporation and secondary pyrolysis reactions of the fuel droplets. The spatial distribution of the oxidation zone and thus local temperature and species concentrations depend on the complex interaction between entrainment of ambient syngas and oxidation of fuel [18]. The oxidation reactions in the burner near zone provide the thermal energy needed for evaporation and endothermal gasification reactions and are known to be important for cracking hydrocarbons [19,20]. It is known from literature that under typical EFG conditions, a significant portion of fuel does not evaporate in the high temperature oxidation zone [1,2,21], leading to a conversion of fuel droplets further downstream in a moderate temperature environment under fuel rich conditions. Links between evaporation and pyrolysis processes of fuel particles outside the flame and by-product formation have been proposed [2,5,22]. However, systematic literature on this subject is scarce and rules for burner development for combustion applications are not easily transferable to gasification conditions [5].

In order to fill the mentioned gap of data and to improve the understanding of the fuel conversion processes in the burner near zone, this study aims to quantitatively assess the evaporation of a liquid fuel spray under technically relevant EFG-conditions. The question how much fuel evaporates within the EFG flame and which process parameters exhibit the highest impact on fuel evaporation is addressed. The influences of gas momentum flow, droplet size and spray angle on the evaporation of the surrogate fuel monoethylene glycol (MEG) are examined in a 60 kW EFG unit by detailed optical measurement and modeling. Two burner nozzles featuring different gas exit areas were applied under identical gas and liquid mass flows. The resulting different gas momentum flows at the nozzle exit influence gas phase mixing (i.e. flame shape) and spray (i.e. droplet velocity, spray angle and droplet size). Fuel sprays were characterized under cold and reactive conditions. Droplet size and velocity in the gasification experiment were measured along the jet axis by PDA. The results were used to investigate the evolution of droplet size distribution during the evaporation process as well as for calculating droplet residence times in the oxidation zone. In addition, a qualitative assessment of liquid fuel concentration by Fuel-Tracer-LIF was conducted in order to estimate of the amount of evaporated fuel, providing a detailed data set on fuel conversion under EFG conditions. Experimental results are complemented by a model based investigation of the experimental cases as well as a sensitivity study using a 2-phase free jet model developed by Hotz [23]. Gas momentum flow, droplet size and spray angle were varied independently in order to gain a systematic understanding of parameter sensitivities. Parameter spaces for high and low fuel conversion in the flame zone are identified as a basis for burner development.

2. Methods

2.1. Experimental

Since the experimental facilities used in this study have been elaborated in preceding works, only a brief overview is given here. Two external mixing twin fluid nozzles with a central liquid jet and an annular gas outlet as shown in Fig. 1 were used. The two nozzles differ in the gas outlet diameter d_{gas}, resulting in different gas exit areas and therefore different gas momentum flow. The geometry parameters for the two nozzles are given in Table 1 together with liquid and gas mass flows as well as the resulting gas momentum flows. Due to its chemical composition (C/H/O) similar to biogenic pyrolysis oil and for comparability to other experiments in this series, mono ethylene glycol (MEG) was used as a reference fuel. The nozzles together with their respective experimental data set are defined as case A and case B. Ambient spray characterization experiments with MEG were performed at the Atmospheric Spray Test Rig ATMO, which is described in detail in [24]. PDA

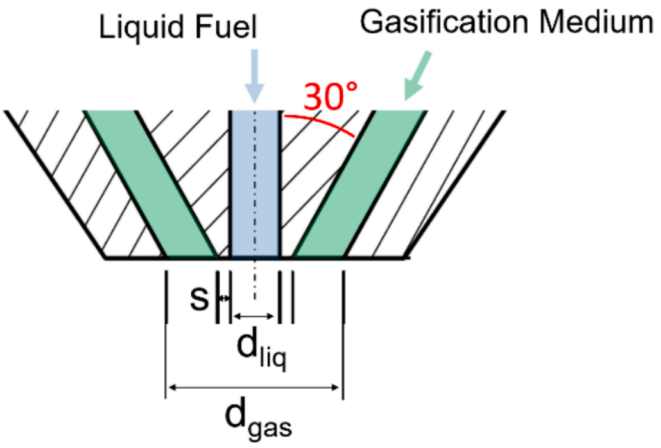

Fig. 1. Geometry of the twin-fluid atomizer nozzles applied in the experiments.

Table 1
Operating conditions and spray data for the two experimental cases.

Quantity	Case A	Case B
$\dot{M}_{fuel}$ / kg/h	12.42	
$\dot{M}_{air}$ / kg/h	3.77	
$\dot{M}_{O2}$ / kg/h	6.55	
d_{liq} / mm	2	
s / mm	0.5	
d_{gas} / mm	7.12	5.25
$u_{0,gas}$ / m/s	69.4	156.0
J_{gas} / kg/m/s^2	0.20	0.45
SMD (integral, z = 100 mm) / µm	160.2	73.1
$\Theta_{0.9}$ (z = 100 mm) / °	40.4 [1]	23.5 [1]

measurements were conducted at axial nozzle distances from 50 mm to 250 mm to measure radial profiles of droplet size for the two investigated cases. A mechanical patternator was used to measure the radial liquid mass flux distribution at the same axial nozzle distances. Based on the radial mass flux distribution, a spray angle $\theta_{0.9}$ containing 90 % of the liquid mass flow was defined. Further details on these measurements and their data evaluation can be found in [1], where the data for z = 100 mm has already been presented. The results of the ambient spray characterization data used as model input are listed in Table 1, the full datasets are provided in the supplementary material. The gasification experiments were conducted at the Research Entrained Flow Gasifier REGA at atmospheric pressure. The plant consists of a tubular reactor with an electrically heated Al_2O_3 ceramic refractory lining featuring optical access ports. A detailed description of the plant is given in [25]. The fuel was gasified with oxygen enriched air under the conditions given in Table 1, resulting in an adiabatic temperature of 1700 °C.

Under reacting conditions, droplet size and droplet velocity were determined using the same PDA system as for the ambient condition experiments. OH and fuel tracer LIF were measured simultaneously from 0 – 300 mm axial nozzle distance in order to determine the spatial distribution of oxidation zone and fuel spray. Rhodamine 6G was used as a fuel tracer in a concentration of 10^{-5} mol/l. Simultaneous excitation of OH radicals and fuel tracer was performed at the $Q_1(8)$ line of the OH radical at a wavelength of 283.55 nm. The fluorescence signal of OH and fuel tracer were recorded in 2 separate channels using an image intensifier equipped with a stereoscope. A 320 nm / 40 nm FWHM bandpass filter was used for the detection of OH while the channel for the fuel tracer LIF signal was equipped with a 572 nm / 33 nm FWHM bandpass filter. Further details on the LIF measurement and the image post-processing are given in [1].

Fuel Tracer LIF is widely applied to characterize non-reacting and reacting sprays and can under certain conditions be used to gain

quantitative information on fuel concentration [26–29]. In this work, the fuel tracer Rhodamine 6G is used which has a negligible vapor pressure and is reported to decompose at temperatures above 219 °C before reaching its boiling point [30]. In accordance with works by other authors [31], it is therefore assumed to mark the liquid phase exclusively. However, the enrichment of fuel tracer in the droplets during the evaporation process together with the temperature dependence of the fluorescence signal of Rhodamine 6G [32,33] allows only a qualitative interpretation of the fuel tracer LIF signal under reacting conditions.

The boundaries of the oxidation zone for the experimental cases were determined using the measured OH-LIF intensities, with the longitudinal extension of the OH zone L_{OH} defined as the axial distance where the OH-LIF signal drops below 10 % of the maximum value [18]. The flame volume V_{OH} is defined analogous by volumetric integration of the 10 % OH contour. See (Table 2).

2.2. Model

For modeling the liquid evaporation processes in the burner near region, a 2-phase free jet model was used. The model was originally developed by Hotz and is in depth described in [23]. The model assumes a 2-phase free jet of gasification medium and fuel spray that mixes with a surrounding hot syngas atmosphere. The model is implemented in MATLAB and features a modular setup [23]. The equations for exchange of momentum, heat and mass for a single phase free jet were modified in order to describe the mixing in the two phase case as outlined in [34], which serves as a basis of the model. Gas and liquid phase are assumed to enter the modeling domain through a circular orifice with an equivalent diameter d_{eq} derived from free jet theory, which also marks the origin of the computational grid described in [23]. The modular setup allows to complement the basic description of the 2-phase jet with sub-models for gas phase reaction, heat and mass transfer and droplet conversion, which are described below.

Due to the high temperatures in the flame zone, gas phase species in each cell are assumed to be in chemical equilibrium and were calculated using a 4 reaction equation approach in the original model. To describe species dissociation to radicals in the high temperature zone and to enable a comparison with the measured OH distributions, the reaction model was revised using a Gibbs free energy minimization approach [18]. The longitudinal extension and volume of the OH distribution in the modeled cases is determined based on the calculated OH number density analogous to the experimental cases described above.

In the model, the droplets move along straight trajectories originating at the nozzle exit and are accelerated according to a momentum balance. Heat transfer between liquid and gas phase as well as droplet evaporation can be described using different droplet models [23]. In order to reflect the radial distribution of liquid mass flux, the original model was modified by Haas as described in [1].

To assess the impact of the droplet evaporation model on the fuel evaporation within the flame zone, two different droplet model approaches were investigated. As a reference, the simple d^2-law was considered. Once a droplet reaches its boiling temperature, its diameter can be described as

$$d^2(t) = d_0^2 - K \bullet t \tag{1}$$

with the initial droplet diameter d_0.The evaporation factor K can be expressed as

$$K = \frac{8\lambda_{gas}}{\rho_{liq}} \bullet B \tag{2}$$

using the gas phase thermal conductivity λ_{gas}, the liquid density ρ_{liq},. The Spalding evaporation factor B is given by

$$B = \frac{\ln\left(1 + c_{p,gas}\frac{T_\infty - T_{liq}}{\Delta h_{vap}}\right)}{c_{p,gas}} \tag{3}$$

with the gas phase heat capacity $c_{p,gas}$, surrounding temperature T_∞ and heat of evaporation Δh_{vap} [7]. The d^2-law uses a quasi-steady-state approach considering only heat conduction. A more accurate description of evaporation also considering convective effects is given by the heat convection limited Spalding approach, which is widely used in droplet evaporation calculations [7]. After a droplet reaches its boiling temperature, the temporal evolution of the droplet mass is in this model described by

$$\frac{dm_{liq}}{dt} = \pi d^2 \bullet \alpha \bullet B \tag{4}$$

using a heat transfer coefficient α determined by a Nusselt correlation. In further contrast to the d^2-law, evaporation before reaching the boiling temperature is modeled by

$$\frac{dm_{liq}}{dt} = \pi d^2 \bullet \beta \bullet \left(C_{vap,s}(T_{liq}) - C_{vap,\infty}\right) \tag{5}$$

with the bulk concentration of fuel vapor $C_{vap,\infty}$ and the concentration of fuel vapor at the droplet surface $C_{vap,s}(T_{liq})$ determined by the vapor pressure curve. The coefficient of mass transfer β is derived from a Sherwood correlation.

Table 2
List of Acronyms.

Glossary	
Acronym	**Description**
2-Ph-FJM	2-Phase Free Jet Model
ATMO	Atmospheric Spray Test Rig
CFD	Computational Fluid Dynamics
EFG	Entrained Flow Gasification
LIF	Laser Induced Fluorescence
MEG	Mono Ethylene Glycol
PDA	Phase-Doppler Anemometry
REGA	Research Entrained Flow Gasifier
SMD	Sauter Mean Diameter

3. Results

The first section 3.1 of this chapter describes the analysis of the qualitative fuel tracer LIF measurement from the gasification experiments and compares the findings regarding fuel evaporation with model data. In the following two sections 3.2 and 3.3, droplet residence time in the OH zone and the evolution of droplet size distribution during evaporation are discussed based on experimental and model data. A model sensitivity study separately investigating the influence of nozzle and spray parameters on fuel evaporation is presented in section 3.4.

3.1. Assessment of fuel evaporation

In order to get a qualitative representation of the liquid fuel distribution under gasification conditions, the fuel tracer LIF signal was measured for case A and B according to the procedure described above. Fig. 2 shows images of absolute LIF intensities (gray scale) together with flame contours from the OH-LIF measurement (red) reported in [1]. The images clearly show distinct spray patterns due to the different gas momentum flow at the nozzle outlet, which also affects the flame. The Fuel-Tracer-LIF signal marking the liquid phase indicates that fuel droplets are found outside the OH contour in both cases.

As shown by the values in Table 1, case A exhibits a lower gas momentum flow at the nozzle exit which results in a reduced entrainment rate of ambient syngas into the free jet causing a larger flame zone indicated by OH. Additionally, the lower gas momentum flow in case A leads to larger droplets and a wider spray angle in comparison to case B.

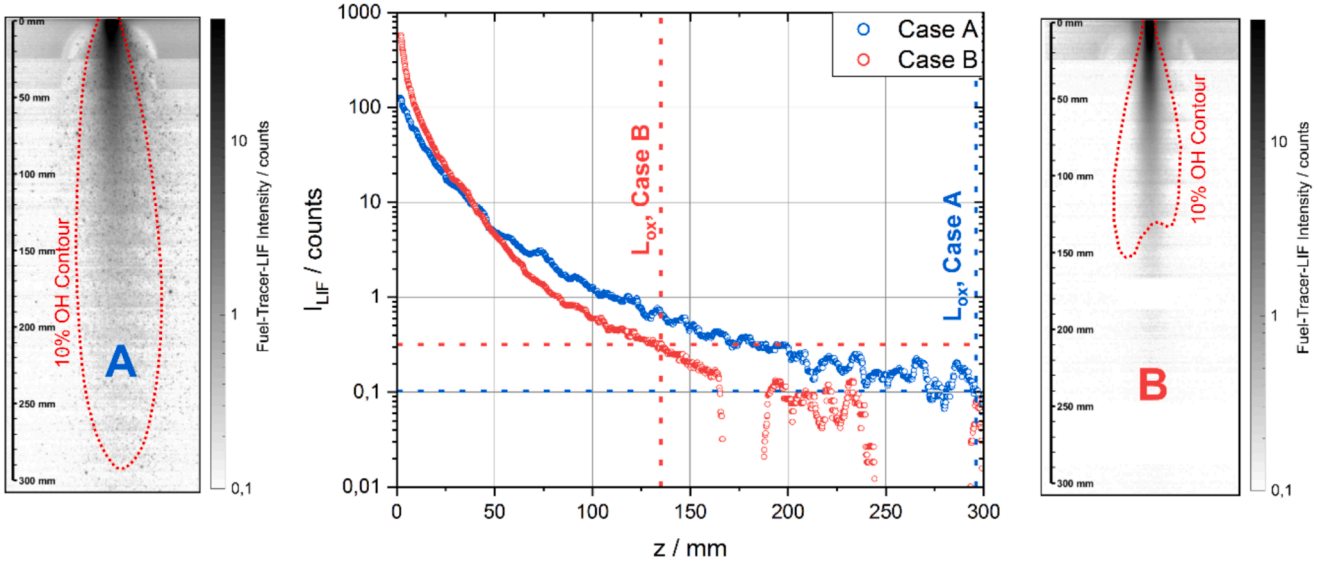

Fig. 2. Measured spray distributions (Fuel Tracer LIF) and flame contours (OH LIF) [1] for cases A and B. Fuel-Tracer-LIF intensities along the jet centerline are shown in the central graph.

For case A, a considerable amount of droplets is visible outside the jet boundaries, which is a consequence of the high spray angle. In case B, the higher gas momentum flow causes a shorter flame zone through enhanced syngas entrainment together with a finer spray and smaller spray angle. In contrast to case A, the remaining fuel outside the OH contour in case B is mostly found at the jet centerline.

Profiles of Fuel-Tracer-LIF intensity I_{LIF} along the jet axis are shown in Fig. 2. Close to the nozzle exit, I_{LIF} is higher for case B. This indicates a higher fuel concentration on the jet axis that is caused by the narrower spray angle. The smaller droplet size in case B allows a faster fuel evaporation, which is indicated by the stronger decrease of LIF intensity along the jet axis in comparison to case A. Since the tracer Rhodamine 6G is assumed to exclusively mark the liquid phase during evaporation without occurring in the gas phase, a lower LIF signal indicates that less liquid fuel is present per volume further downstream the nozzle in case B. At the end of the oxidation zone of case B however, it is apparent that the fuel tracer LIF signal is higher than it is for case A, which is already close to the detection limit at the end of the OH zone.

Because a direct quantitative measurement of the amount of evaporated fuel in the reacting system is not possible due to the diagnostic limitations discussed in section 2.1, data obtained by the 2-Ph-FJM is used for further investigation. Fig. 3 shows the calculated evaporation progress as fraction of evaporated fuel $x_{liq,vap,jet}$ along the jet axis. Case B shows a larger fraction of evaporated fuel at a given nozzle distance due to the smaller droplet size, which is in agreement with the insights gained from the LIF data shown in Fig. 2. Due to the larger OH zone and the longer droplet residence time in case A, the model shows a higher fuel evaporation progress at the end of the oxidation zone in case A which is also in agreement with observations made before. As this result shows, the fraction of fuel evaporating within the OH zone is controlled by the competing influence of droplet size and droplet residence time, which will be studied in more detail in the next two chapters. The overall calculated evaporation progress on the jet centerline within L_{OH} is $x_{liq,vap,jet}$ = 25 % for case A and $x_{liq,vap,jet}$ = 13 % for case B. Additional validation data comparing the measured LIF intensities with modeled droplet concentrations are given in the supplementary material.

Because the two cases exhibit different spray angles, the total evaporation within the flame volume defined by the OH contour must be taken into account. The model calculations show a total amount of evaporated fuel mass within the flame volume of $x_{liq,vap}$ = 15 % (case A)

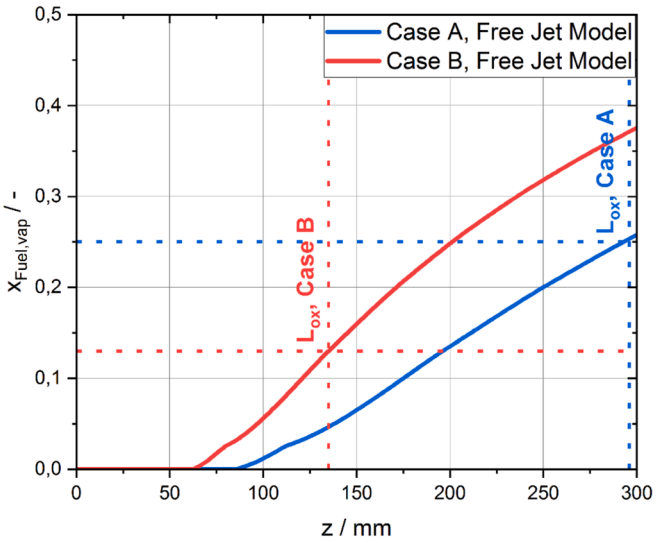

Fig. 3. Evaporated mass fraction of fuel on the jet centerline $x_{liq,vap,jet}$ for cases A and B calculated by the free jet model using the d^2-law.

and of $x_{liq,vap}$ = 22 % (case B) using the d^2-law as evaporation model (of $x_{liq,vap}$ = 23 % and 32 % respectively for the heat transfer controlled Spalding model). The impact of spray angle on droplet evaporation under EFG conditions is further discussed in section 3.4. This result clearly shows that in both cases the major fraction of the fuel does not evaporate within the oxidation zone. These fuel droplets are converted in a syngas atmosphere under moderate temperatures, which may have a major impact on the formation of by-products during gasification [22,35].

3.2. Droplet residence time in flame zone

The differences in droplet residence time for the two cases are further investigated in this chapter. Experimental mass averaged droplet residence times have been determined using droplet mass averaged axial velocities measured along the jet axis by PDA in the gasification experiment (Fig. 4). For both cases, droplet residence times derived from

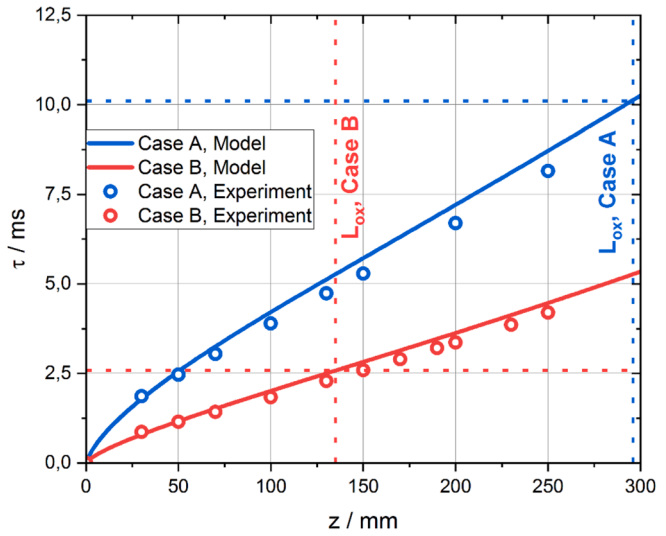

Fig. 4. Droplet residence time along the jet axis determined from the PDA under gasification conditions data together with modelled residence times.

model data agree well with the experimental data. Case A shows a steeper increase of droplet residence time along the jet axis than case B. This is caused by the lower gas momentum flux in case A leading to slower droplets and thus an increased time for the droplets to reach a given nozzle distance z. The lower gas momentum flux also leads to slower mixing of ambient medium into the free jet, which increases the longitudinal extension of the OH zone L_{OH}. This causes a twofold increase of droplet residence time within L_{OH} in case A ($\tau =$ 10.1 ms) in comparison to case B ($\tau =$ 2.5 ms). The longer residence time allows more fuel to evaporate within the oxidation zone, as indicated by the experimental and modeling results above. For both cases, droplet residence times in the oxidation zone are in the order of few milliseconds, explaining the incomplete fuel evaporation in the oxidation zone observed above. The results show that the gas momentum flow at the nozzle exit can have a strong influence on the amount of fuel evaporated within the oxidation zone, with a large gas exit area supporting fuel evaporation.

3.3. Evolution of droplet size distribution in flame zone

In order to assess the influence of droplet size on evaporation in the EFG flame, modeling results for case A using the d^2-law are presented in Fig. 5. A selection of droplet size classes of the droplet collective along the jet axis is shown with droplet diameters normalized to their initial diameter. In this case, heating of droplets starts at the end of the core zone of the jet at an axial distance of about 71 mm, leading to an initial increase in droplet diameter due to the reduction of liquid density with temperature. After complete heat up to the boiling point, droplet diameters decrease following the d^2-law. The smallest droplet class shown in the graph fully evaporates shortly after the start of droplet heating within a nozzle distance of 103 mm. Larger droplets take a longer distance to heat up and evaporate. According to the model results applying the d^2-law, the largest droplet class to fully evaporate within the OH zone has a diameter of 59,8 µm. Droplet classes larger than that take considerably longer to heat up and show only a small decrease in droplet size within L_{OH}, showing that only a small amount of fuel is released by these larger droplets within the oxidation zone. These large droplets are most prevalent to evaporate in the post flame zone and may contribute to the formation of unwanted by-products during gasification.

These findings are in agreement with the experimentally determined droplet size distributions measured for case A along the jet axis by PDA (Fig. 6). With increasing nozzle distance, SMD increases as small droplets are consumed by evaporation and large droplets remain in the spray. If a more complete droplet evaporation within the OH zone is desired, it is thus necessary to reduce the amount of large droplets formed in the atomization process.

3.4. Model sensitivity study on fuel evaporation

The results above show that droplet size distribution, spray angle and droplet residence time influence the amount of fuel evaporated within the OH zone. Since these parameters are all affected by the gas momentum flux at the nozzle exit, they can not be separately investigated in the experiment. Therefore a sensitivity study applying the 2-phase free jet model was conducted. For simplicity, the spray angle was kept constant and identical to the gas jet angle in the first set of calculations discussed here. For the operating conditions used in the experiment, droplet size distributions with SMD between 50 µm and 400 µm and equivalent nozzle diameters d_{eq} ranging from 4 mm to 10 mm were used as input conditions. At each point, a droplet collective with a Weibull droplet size distribution using 50 droplet size classes was considered. The fraction of fuel evaporated within the OH zone $x_{liq,vap}$ was determined by integrating the fuel evaporation over the flame volume derived from the OH radical distribution. As described earlier, the two

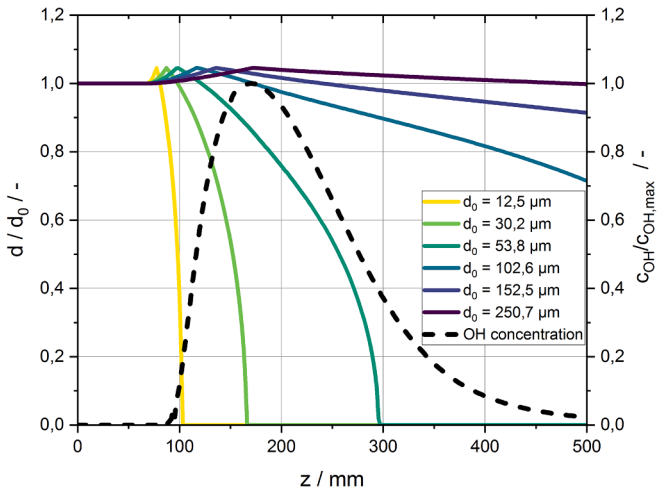

Fig. 5. Calculated normalized droplet diameter on the jet axis for selected droplet size classes of the droplet collective displayed together with the axial OH profile (Case A, d^2-law).

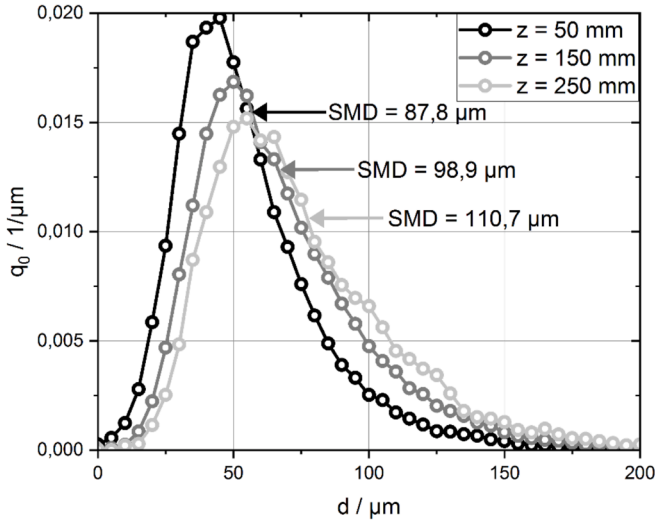

Fig. 6. Droplet size distribution on the jet centerline measured by PDA (Case A).

evaporation models from section 2.2 were compared. The results are displayed in Fig. 7.

For constant SMD, an increase in nozzle equivalent diameter d_{eq} (decrease in gas momentum flow) causes an increase in the amount of fuel evaporated within the OH zone, which is in agreement with the observations reported above. The lower gas momentum flow leads to slower droplets and a longer OH zone, which results in a twofold increase of droplet residence time within the OH zone, leading to a higher amount of fuel being able to evaporate. For a given gas momentum flow, the fraction of fuel evaporated in the OH zone can be further increased by a lowering the SMD, which is also expected from the prior experimental results. This effect is very pronounced for all gas momentum flows investigated.

The model comparison shows that for all points investigated, the heat convection controlled evaporation model yields higher values for $x_{liq,vap}$ than the d^2-law, which only takes into account heat conduction.

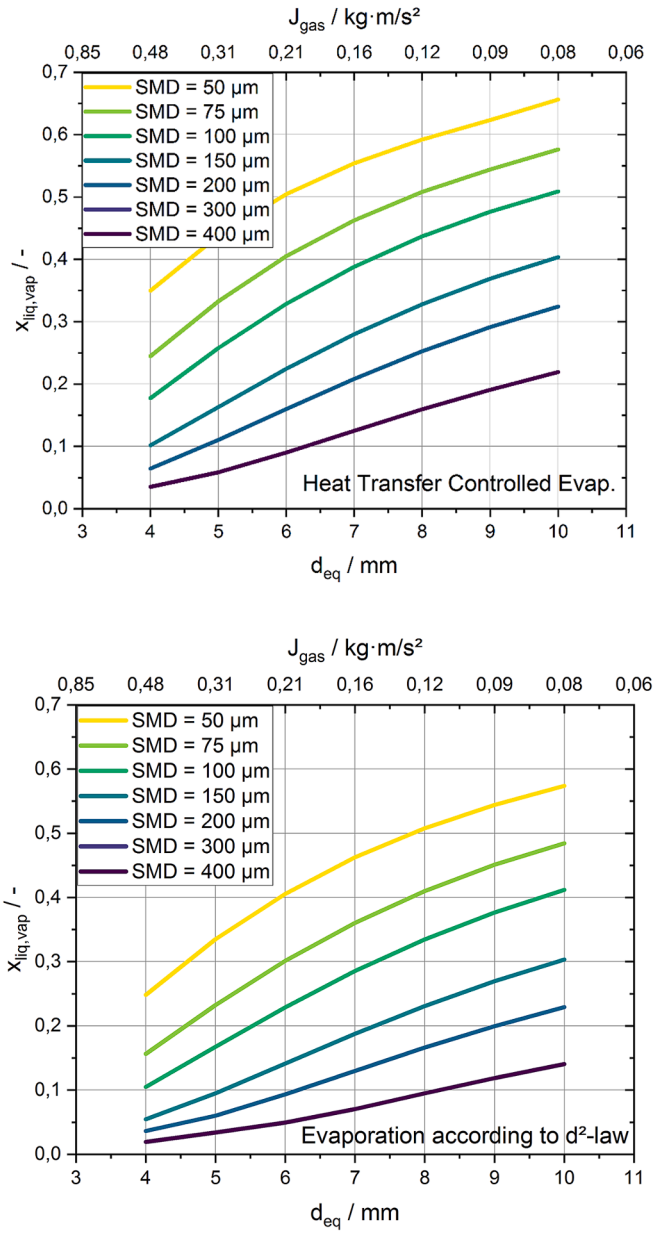

Fig. 7. Calculated mass fraction of fuel evaporated in the OH zone volume for different values of nozzle equivalent diameter and SMD. The spray angle is equivalent to the gas jet angle. The droplet evaporation using d^2-law is compared to the heat transfer controlled Spalding approach.

The individual values however do not differ by much, showing that the simple d^2-law can give a reasonable approximation.

The results above show that a low gas momentum at the nozzle exit combined with a small droplet size favors fuel evaporation within the oxidation zone. In a technical twin-fluid atomizer nozzle, gas momentum flow and SMD cannot be controlled independently because the atomization process is influenced by the gas momentum flow itself. Typically, an increase in d_{eq} (reduction of gas momentum flow) would on the one hand lead to a longer residence time in the oxidation zone, but would on the other hand lead to larger droplets, resulting in two opposing effects on the amount of fuel evaporated in the oxidation zone. A general conclusion for a technical system would therefore require knowledge about the dependence of droplet size on gas momentum for the used burner type in a broad range in form of a theoretical prediction or an empirical correlation. This makes further research in the area of fuel atomization necessary.

The impact of spray angle on fuel evaporation within the OH zone is visualized in. Fig. 8. Here, the process conditions from the experimental cases were used as input for the model under variation of droplet size distribution characterized by SMD in the range of 50 – 400 µm and spray

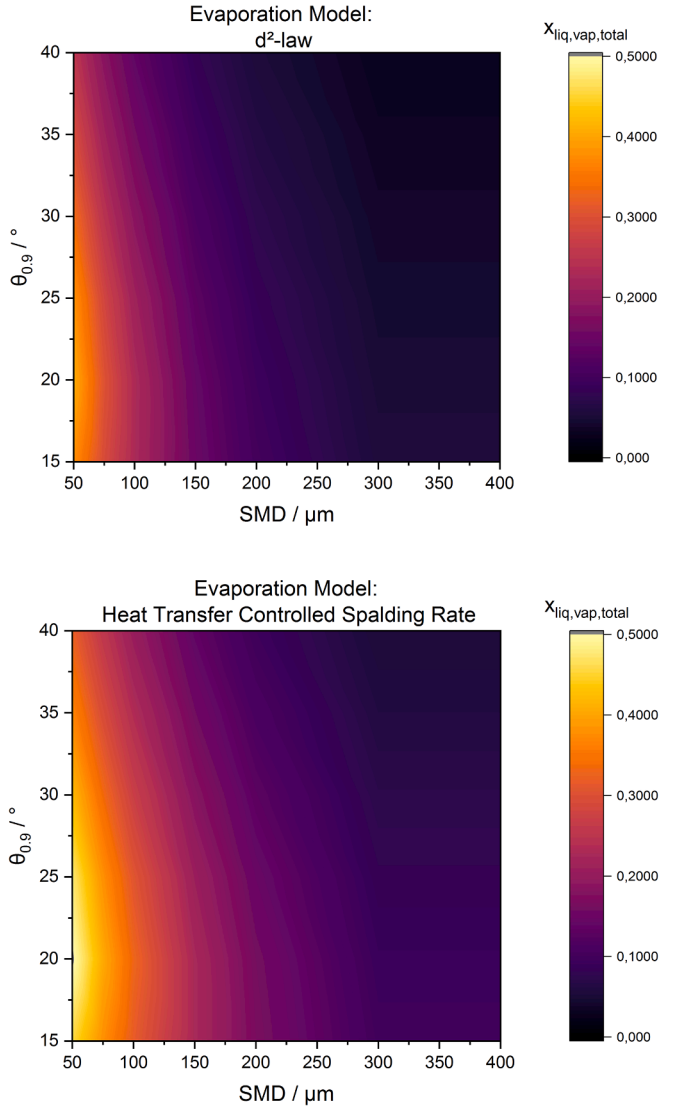

Fig. 8. Total amount of evaporated liquid fuel within the flame boundaries calculated for different spray angles and droplet size distributions applying 2 different evaporation models. A constant nozzle equivalent diameter d_{eq} = 6 mm was assumed.

angle $\theta_{0,9}$ between 15° − 40°. The sensitivity analysis was performed with a constant nozzle diameter $d_{eq} = 6$ mm. For each point, the amount of liquid evaporation within the OH zone $x_{liq,vap}$ was calculated. As shown above, an increase of SMD reduces fuel evaporation in all cases. For a given initial droplet size distribution, it can be observed that the highest $x_{liq,vap}$ is achieved at spray angles around 20°, which roughly corresponds to the gas free jet angle. In this configuration, the distribution of fuel within the OH zone is found to be optimal for evaporation. For higher spray angles, $x_{liq,vap}$ is reduced because more fuel is present on trajectories outside the gas jet that does not come in direct contact with the high temperature oxidation reactions marked by OH, which is the situation found in the experimental case A (see Fig. 2).

For spray angles smaller than the gas free jet angle, a reduction of, $x_{liq,vap}$ is also found compared to $\theta_{0,9} = 20°$. Under these conditions, the concentration of liquid fuel on the jet centerline is very high, leading to low local temperatures and stoichiometries, [1]. This causes a large portion of the fuel to traverse the flame zone at the jet axis, which is the situation found in experimental case B. (see Fig. 2). In order to link these results to EFG process performance, further knowledge on the conversion behavior of the droplets outside the flame is required.

The model comparison again shows that in all cases, a higher amount of liquid fuel evaporates when the heat convection controlled evaporation approach is used. The qualitative trends however are the same for both models.

4. Conclusion

The situation in the burner near region of EFG reactors for liquid fuels can be described as an inverse diffusion flame of oxygen rich gasification medium reacting with hot syngas entrained from the environment, which is superimposed by a central fuel spray. Since reactants are usually fed to the system using twin-fluid atomizer nozzles, the gasification medium also serves as atomization medium. As a consequence, the momentum flow of the gasification medium does not only determine flame structure but also spray parameters (i.e. spray angle, droplet velocity and droplet size).

This study investigates the evaporation of a liquid surrogate fuel (MEG) in the burner near region of an atmospheric pressure EFG unit. Fuel evaporation is compared for two twin-fluid atomizer nozzles with different gas exit area. Gas and liquid mass flow are kept constant, thus gas momentum flow is varied. PDA and Fuel-Tracer LIF are used to measure droplet size, droplet velocity and qualitative data on fuel spray distribution under reacting conditions for both cases while OH-LIF is used to measure the flame structure. A 2-phase free jet model is applied to interpret the experimental data. In addition, a sensitivity study on the influence of gas momentum, spray angle and droplet size on the amount of fuel evaporated in the high temperature oxidation zone is conducted. The impact of the liquid evaporation model is investigated by comparing the simple d^2-law with a heat transfer limited Spalding approach.

The model results show good agreement with the experimental data. A major portion of fuel was found to evaporate outside the flame boundaries in both cases. Experimental and model results indicate a strong impact of droplet residence time and spray parameters on the amount of fuel evaporation within the flame boundaries. High droplet residence times caused by a low gas momentum flow together with small droplets and a spray angle similar to the gas free jet angle were found to be beneficial for fuel evaporation within the flame zone.

The 2-Ph FJM allows to investigate the flame detached from the integral system and shows the capability to describe the parameter sensitivities in the investigated flame type. In order to quantify the impact of these effects on EFG process performance, more complex models and further experimental work are needed, especially to characterize the impact of the fuel conversion reactions within and outside the flame zone on by-product formation. With further understanding of this subject provided, the 2-Ph FJM can be used to define boundary conditions for the development of burners for larger scale EFG units and for CFD reactor simulations.

Declaration of Generative AI and AI-assisted technologies in the writing process

During the preparation of this work the authors used no generative AI tools.

CRediT authorship contribution statement

Manuel Haas: Writing – original draft, Validation, Software, Methodology, Investigation, Conceptualization. **Sabine Fleck:** Writing – review & editing, Supervision, Project administration, Investigation, Conceptualization. **Tobias Jakobs:** Writing – review & editing, Methodology. **Thomas Kolb:** Writing – review & editing, Supervision.

Declaration of competing interest

The authors declare that they have no known competing financial interests or personal relationships that could have appeared to influence the work reported in this paper.

Acknowledgments

This work was funded by the Helmholtz Association of German Research Centers (HGF) in the context of the research program Materials and Technologies for the Energy Transition (MTET). The authors thank Juliana Richter (Karlsruhe Institute of Technology, Institute for Technical Chemistry, Gasification Technology) and Simon Wachter (formerly Karlsruhe Institute of Technology, Institute for Technical Chemistry, Gasification Technology) for providing experimental facilities and support for the spray characterization experiments.

Appendix A. Supplementary data

Supplementary data to this article can be found online at https://doi.org/10.1016/j.tsep.2025.103342.

Data availability

Data will be made available on request.

References

[1] M. Haas, M. Dammann, S. Fleck, T. Kolb, Entrained flow gasification: Impact of fuel spray distribution on reaction zone structure, Fuel 334 (4) (2023) 126572, https://doi.org/10.1016/j.fuel.2022.126572.
[2] A. Bader, M. Hartwich, A. Richter, B. Meyer, Numerical and experimental study of heavy oil gasification in an entrained-flow reactor and the impact of the burner concept, Fuel Process. Technol. 169 (2018) 58–70, https://doi.org/10.1016/j.fuproc.2017.09.003.
[3] N. Fang, Y. Lu, Z. Li, Y. Lu, Z. Chen, Improving mixing and gasification characteristics in an industrial-scale entrained flow gasifier with a novel burner, J. Clean. Prod. 362 (2022) 132157, https://doi.org/10.1016/j.jclepro.2022.132157.
[4] J. Lee, S. Park, H. Seo, M. Kim, S. Kim, J. Chi, et al., Effects of burner type on a bench-scale entrained flow gasifier and conceptual modeling of the system with Aspen Plus, Korean J. Chem. Eng. 29 (5) (2012) 574–582, https://doi.org/10.1007/s11814-011-0217-z.
[5] Y. Ögren, M. Gullberg, J. Wennebro, A. Sepman, P. Tóth, H. Wiinikka, Influence of oxidizer injection angle on the entrained flow gasification of torrefied wood powder, Fuel Process. Technol. 181 (2) (2018) 8–17, https://doi.org/10.1016/j.fuproc.2018.09.005.
[6] P.A. Nikrityuk, B. Meyer, Gasification processes: Modeling and simulation, John Wiley & Sons, 2014.
[7] S. Sazhin, Droplets and Sprays, Springer, London, London, 2014.
[8] W.A. Sirignano, Fuel droplet vaporization and spray combustion theory, Prog. Energy Combust. Sci. 9 (4) (1983) 291–322, https://doi.org/10.1016/0360-1285(83)90011-4.
[9] M. Broumand, S. Albert-Green, S. Yun, Z. Hong, M.J. Thomson, Spray combustion of fast pyrolysis bio-oils: applications, challenges, and potential solutions, Prog.

Energy Combust. Sci. 79 (2020) 100834, https://doi.org/10.1016/j.pecs.2020.100834.
[10] H. Chiu, Advances and challenges in droplet and spray combustion. I. Toward a unified theory of droplet aerothermochemistry, Prog. Energy Combust. Sci. 26 (4–6) (2000) 381–416, https://doi.org/10.1016/S0360-1285(00)00016-2.
[11] P. Jenny, D. Roekaerts, N. Beishuizen, Modeling of turbulent dilute spray combustion, Prog. Energy Combust. Sci. 38 (6) (2012) 846–887, https://doi.org/10.1016/j.pecs.2012.07.001.
[12] J. Warnatz, U. Maas, Dibble RW. Combustion. [New York]: Springer-Verlag Berlin Heidelberg; 2006.
[13] H. Chiu, T.M. Liu, Group combustion of liquid droplets, Combust. Sci. Technol. 17 (3–4) (1977) 127–142, https://doi.org/10.1080/00102207708946823.
[14] V.G. McDonell, G.S. Samuelsen, Measurement of fuel mixing and transport processes in gas turbine combustion, Meas. Sci. Technol. 11 (7) (2000) 870–886, https://doi.org/10.1088/0957-0233/11/7/304.
[15] J. Hayashi, H. Watanabe, R. Kurose, F. Akamatsu, Effects of fuel droplet size on soot formation in spray flames formed in a laminar counterflow, Combust. Flame 158 (12) (2011) 2559–2568, https://doi.org/10.1016/j.combustflame.2011.05.015.
[16] R. Borghi, The links between turbulent combustion and spray combustion and their modelling, in: 8Th International Symposium on Transport Phenomena in Combustion, 1996, pp. 1–18.
[17] G. Eckel, P. Le Clercq, T. Kathrotia, A. Saenger, S. Fleck, M. Mancini, et al., Entrained flow gasification. Part 3: insight into the injector near-field by Large Eddy Simulation with detailed chemistry, Fuel 223 (2018) 164–178, https://doi.org/10.1016/j.fuel.2018.02.176.
[18] M. Haas, C. Hotz, S. Fleck, T. Kolb, Analysis of Burner Near Field in an Entrained Flow Gasifier applying a 2-Phase Free Jet Model and Optical Diagnostics: (in preparation) 2025.
[19] C. Higman, M. van der Burgt, Gasification, Elsevier, 2003.
[20] F. Weiland, P.T. Nilsson, H. Wiinikka, R. Gebart, A. Gudmundsson, M. Sanati, Online characterization of syngas particulates using aerosol mass spectrometry in entrained-flow biomass gasification, Aerosol Sci. Tech. 48 (11) (2014) 1145–1155, https://doi.org/10.1080/02786826.2014.965772.
[21] Z. Xue, Q. Guo, Y. Gong, X. Wu, F. Wang, G. Yu, Detailed deposition characteristics around burner plane in an impinging entrained-flow coal gasifier, Chem. Eng. Sci. 198 (2019) 85–97, https://doi.org/10.1016/j.ces.2019.01.016.
[22] J. Simonsson, H. Bladh, M. Gullberg, E. Pettersson, A. Sepman, Y. Ögren, et al., Soot concentrations in an atmospheric entrained flow gasifier with variations in fuel and burner configuration studied using diode-laser extinction measurements, Energy Fuels 30 (3) (2016) 2174–2186, https://doi.org/10.1021/acs.energyfuels.5b02561.
[23] C. Hotz, M. Haas, S. Wachter, S. Fleck, T. Kolb, Two-phase free jet model of an atmospheric entrained flow gasifier, Fuel 304 (21–23) (2021) 121392, https://doi.org/10.1016/j.fuel.2021.121392.
[24] T. Jakobs, N. Djordjevic, S. Fleck, M. Mancini, R. Weber, T. Kolb, Gasification of high viscous slurry R&D on atomization and numerical simulation, Appl. Energy 93 (2012) 449–456, https://doi.org/10.1016/j.apenergy.2011.12.026.
[25] S. Fleck, U. Santo, C. Hotz, T. Jakobs, G. Eckel, M. Mancini, et al., Entrained flow gasification Part 1: gasification of glycol in an atmospheric-pressure experimental rig, Fuel 217 (2018) 306–319, https://doi.org/10.1016/j.fuel.2017.12.077.
[26] T.D. Fansler, S.E. Parrish, Spray measurement technology: a review, Meas. Sci. Technol. 26 (1) (2015) 12002, https://doi.org/10.1088/0957-0233/26/1/012002.
[27] T.D. Fansler, M.C. Drake, B. Gajdeczko, I. Düwel, W. Koban, F.P. Zimmermann, et al., Quantitative liquid and vapor distribution measurements in evaporating fuel sprays using laser-induced exciplex fluorescence, Meas. Sci. Technol. 20 (12) (2009) 125401, https://doi.org/10.1088/0957-0233/20/12/125401.
[28] K. Jung, H. Koh, Y. Yoon, Assessment of planar liquid-laser-induced fluorescence measurements for spray mass distributions of like-doublet injectors, Meas. Sci. Technol. 14 (8) (2003) 1387–1395, https://doi.org/10.1088/0957-0233/14/8/326.
[29] P.G. Felton, F.V. Bracco, M.E.A. Bardsley, On the quantitative application of exciplex fluorescence to engine sprays, J. Engines (1993) 1254–1262.
[30] S. Qiu, H. Chu, Y. Zou, C. Xiang, H. Zhang, L. Sun, et al., Thermochemical studies of Rhodamine B and Rhodamine 6G by modulated differential scanning calorimetry and thermogravimetric analysis, J. Therm. Anal. Calorim. 123 (2) (2016) 1611–1618, https://doi.org/10.1007/s10973-015-5055-5.
[31] I. Düwel, J. Schorr, J. Wolfrum, C. Schulz, Laser-induced fluorescence of tracers dissolved in evaporating droplets, Appl. Phys. B Lasers Opt. 78 (2) (2004) 127–131, https://doi.org/10.1007/s00340-003-1378-1.
[32] P. Bojarski, A. Matczuk, C. Bojarski, A. Kawski, B. Kukliński, G. Zurkowska, et al., Fluorescent dimers of rhodamine 6G in concentrated ethylene glycol solution, Chem. Phys. 210 (3) (1996) 485–499, https://doi.org/10.1016/0301-0104(96)00141-3.
[33] Y. Zhu, O.C. Mullins, Temperature dependence of fluorescence of crude oils and related compounds.
[34] C. Hotz, M. Haas, S. Wachter, S. Fleck, T. Kolb, C. Hotz, et al., Experimental investigation on entrainment in two-phase free jets. Fuel 2023;335(21–23): 126912. https://doi.org/10.1016/j.fuel.2022.126912.
[35] B. Göktepe, K. Umeki, A. Hazim, T.S. Lundström, R. Gebart, Soot reduction in an entrained flow gasifier of biomass by active dispersion of fuel particles, Fuel 201 (2017) 111–117, https://doi.org/10.1016/j.fuel.2016.09.039.